Journal of GeoEngineering, Vol. 12, No. 3, pp. 129-135, September 2017
http://dx.doi.org/10.6310/jog.2017.12(3).4

DYNAMIC SHEAR MODULUS OF THREE RECONSTITUTED SOILS FROM PANZHIHUA IRON TAILING DAM

Wei Li [1], and Kostas Senetakis [2*]

ABSTRACT

In the study, the small-strain shear modulus of three different soils from a tailing dam from China was studied incorporating lateral and vertical bender element inserts in a stress path triaxial apparatus. This allowed the study of the fabric anisotropy of the samples measuring different components of shear modulus. The study reports on the small-strain behavior of the tailing soils discussing sample preparation method effects as well as comparing the response of the samples with respect to literature expressions developed from tests on quartz type sands.

Key words: Tailing soil, shear modulus, fabric anisotropy, sample preparation method, bender elements, particle shape, iron tailings, tailing dam.

1. INTRODUCTION

The evaluation of the geotechnical properties of tailing soils is of major interest for the mining industry, particularly considering that there have been reported many failures of tailing dams over the past decades which have resulted in economic, social and environmental impact to local societies and internationally (Davies and Lighthall 2001; WISE 2014). An important step in understanding the behavior of tailing soils and modeling their geotechnical properties is the study of their small-strain shear modulus. Such measurements in the laboratory necessitate the conduction of resonant column or bender element tests (Richart *et al.* 1970; Ishihara 1996; Clayton 2011) particularly capturing their behavior at strains below 10^{-3}%. Small-strain shear modulus ($G_{\max}$) is an essential soil property in earthquake engineering studies and the deformation prediction of geo-materials. $G_{\max}$ is linked to shear wave velocity (V_s), thus the liquefaction assessment of geo-structures and soils (Kramer 1996). Experience shows that tailing dams may be highly susceptible to liquefaction (Robertson 2010) due to their saturated and relatively loose states and their non-plastic composition of silt to sand-sized grains. Thus, modeling of $G_{\max}$ is an important step in seismic hazard analyses for tailing dams.

In this study, results from bender element tests conducted on three different soils taken from a tailing dam from China are reported with particular focus on the following aspects: (i) study of the fabric anisotropy of the samples and the role of sample preparation method (ii) study of the sensitivity of modulus to pressure and (iii) comparison of the measured moduli from the three tailing soils with expressions proposed in the literature. Note that in this case, an expression proposed in the literature on the basis of experiments on quartz type sands is used (Payan *et al.* 2016), whilst the tailing soils of the study are composed predominantly of complex silicate minerals and some iron minerals.

2. MATERIALS AND METHODS

2.1 Tailing Soils Used in the Study and Their Characterization

The study focused on three different soils from silt to sand size which consisted of Iron tailings from Panzhihua, China. The three different soils corresponded to different grading characteristics (Fig. 1) and were taken from different locations of the tailing dam. The coarser material of sand size was taken from the upper beach (denoted as UB), one silt sized material was taken from the middle beach (denoted as MB) and the finer silt sized material was taken from the pond of the tailing dam (denoted as PO). Table 1 gives a summary of the basic characteristics of the three soils including their mean grain size (d_{50}), coefficient of uniformity (C_u), coefficient of curvature (C_c) and specific gravity of solids (G_s). The particle size distribution of the sands was evaluated with wet sieving and hydrometer analyses. Note the relatively high values of G_s, which ranged between about 3.1 and 3.4 for the three tailing soils, whereas in typical quartz type silts and sands, G_s would have values between about 2.64 to 2.67. These high G_s values are because of the presence of metal minerals within the mass of the tailing soils. A summary of the basic minerals of the three soils is given in Table 1. Based on X-ray diffraction analysis (XRD), the dominant elements were pyroxene (diopside), feldspar (labradorite) and hornblende. A typical graph illustrating the mineral composition of the UB tailing, based on the XRD analysis is given in Fig. 2. Even though, the XRD analysis showed some relative discrepancy of the content of the variable minerals between the different soils, all the soils had in general similar composition.

In the analysis of small-strain shear modulus of soils, particularly of non-plastic geo-materials, which is the focus of this study, the shape of the grains has a dominant role (Cho *et al.* 2006; Senetakis *et al.* 2012; Payan *et al.* 2016). In the study, the

---

Manuscript received January 23, 2017; revised May 30, 2017; accepted June 1, 2017.

[1] Ph.D. student, Department of Architecture and Civil Engineering, City University of Hong Kong, Hong Kong SAR.

[2] Assistant Professor (corresponding author), Department of Architecture and Civil Engineering, City University of Hong Kong, Hong Kong SAR (e-mail: ksenetak@ cityu.edu.hk).

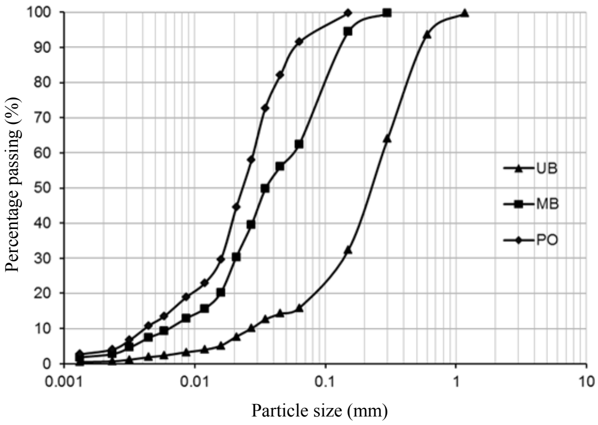

Fig. 1 Grading curves of the three tailing soils of the study

Table 1 Characteristics and composition of tailing soils

Tailings type	Iron (UB)	Iron (MB)	Iron (PO)
d_{50} (mm)	0.220	0.035	0.023
C_u	10.4	10	6.7
C_c	2.6	1.1	2.2
G_s	3.365	3.137	3.112
S	0.66	0.58	0.66
R	0.30	0.34	0.34
ρ	0.48	0.46	0.50
Diopside (%)	30.2	46.1	28.3
Labradorite (%)	32.3	40.2	24.1
Hornblende (%)	11.3	5.5	21.5

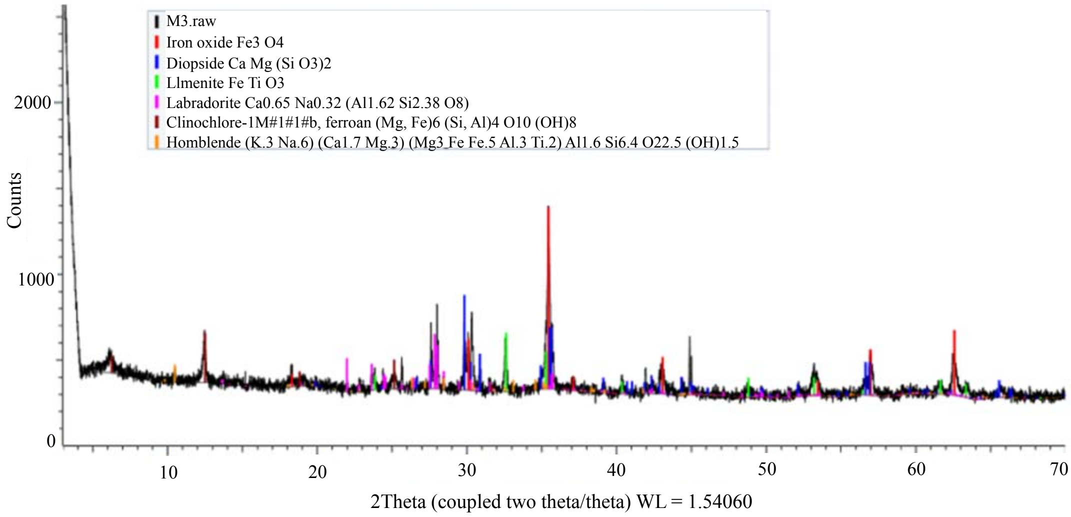

Fig. 2 Typical XRD analysis quantifying the mineral composition of the tailing soils (the example corresponded to sample UB)

particle shape was quantified based on scanning electron microscopy (SEM) image analysis in order to magnify and better observe the grain morphology. Typical images for the UB, MB and PO tailing soils are given in Fig. 3. Three particle shape descriptors, named the sphericity (S), roundness (R) and regularity (ρ) were quantified by visually observing the grains from the SEM images and using an empirical chart proposed by Krumbein and Sloss (1963). Note that the descriptor (ρ), introduced by Cho *et al.* (2006), is the arithmetic mean of sphericity and roundness. As shown in their studies by Cho *et al.* (2006) and Payan *et al.* (2016), soil modulus (or shear wave velocity) is better correlated with the regularity which captures both the roundness and sphericity of the grains. For the purpose of this study, a representative set of grains was examined from each type of soil and two different operators quantified the shape descriptors (S), (R) and (ρ) for the three tailing soils, similar to the procedure described by Payan *et al.* (2016). For each grain examined throughout this process, specific values of the descriptors (S), (R) and (ρ) were evaluated based on the empirical chart by Krumbein and Sloss (1963) and from a total set of about thirty grains for each given tailing sand (*i.e.*, UB, MB or PO), average values of the particle shape descriptors were computed. The average values from this analysis for the different soils are summarized in Table 1. Note the relatively low values of the shape descriptors, particularly for roundness, which implies that the grains of the tailing soils are fairly irregular in shape.

2.2 Equipment, Sample Preparation and Testing Program

A stress path triaxial apparatus of the Bishop and Wesley type (Bishop and Wesley 1975) was used in the study. The apparatus accommodates samples of 50 mm in diameter and 100 mm in length and houses vertical and *T*-shaped lateral bender elements. The vertical bender elements were directly embedded into the top and bottom platens and the *T*-shaped lateral bender elements were mounted on the middle height of the sample. These bender elements could measure the small-strain moduli under three types of shear waves (*S*-waves) propagation: G_{vh} propagating vertically and polarizing horizontally the *S*-waves, G_{hv} propagating horizontally and polarizing vertically the *S*-waves and G_{hh} propagating and polarising horizontally the *S*-waves. G_{vh} was measured with the vertical bender elements, whilst G_{hv} and G_{hh} were measured with the lateral bender elements. The exciting voltage used was 10V and the type of input shear wave was sinusoidal (single cycle). A close-up view of a specimen during its setup with view of the instrumentation with lateral bender elements as well as local strain displacement sensors (LVDTs) is given in Fig. 4. Note that the local strain LVDTs instrumentation incorporates both local axial strain and local radial strain measurements of the samples which was important in the study particularly because a set of specimens was tested in a dry state and there were no measurements of back volume of the samples in a straightforward way as it happens in fully saturated samples.

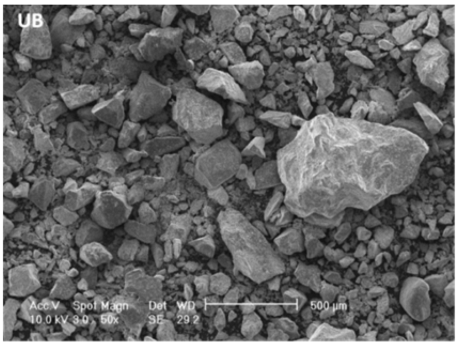

(a) UB

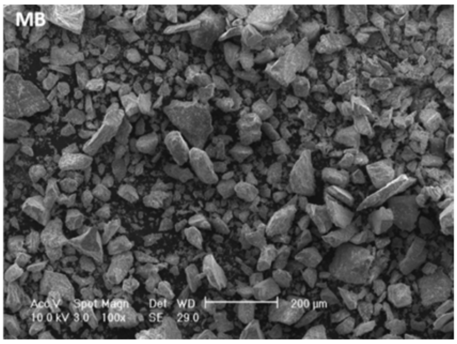

(b) MB

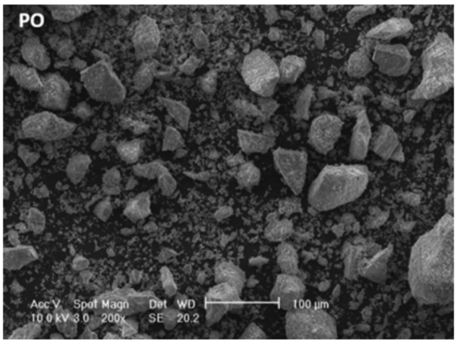

(c) PO

Fig. 3 SEM images of the three tailing soils

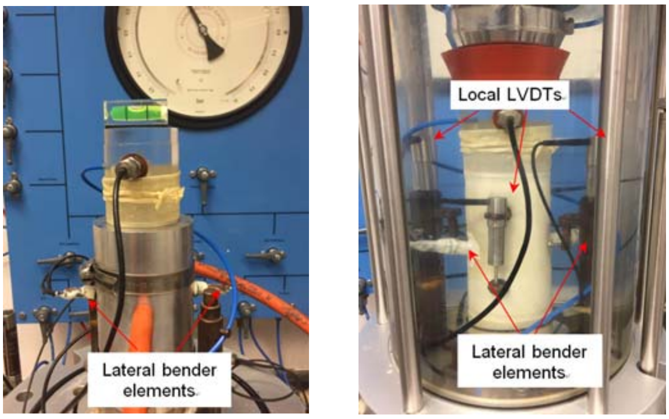

(a) Installation of lateral bender elements (b) Sample ready for measurement

Fig. 4 Sample equipped with lateral bender elements

Previous works have indicated that the behavior of soils, may be affected by the preparation method adopted during the construction of specimens, which results in fabric effects (Ishihara 1993; Yang *et al*. 2008 among others). In this study, all the samples were prepared as reconstituted into a split mold of 50 mm internal diameter and 100 mm in length using two different methods for specimen preparation. One method consisted of the under-compaction (Ladd 1978) and the second one was the slurry method. Using the under-compaction method, the specimen was prepared in a dry state in five layers pouring the material from a small height from the free surface of the sample with subsequent compaction using a steel rod. The top layers were compacted with greater effort in order to achieve more uniform density of the sample along its longitudinal axis (Ladd 1978). Using the slurry method, after the mixing process of the soil with distilled water in a bowl, the slurry sample was placed into a vacuum desiccator to remove the trapped air, prior to the construction of the specimen on the base pedestal of the apparatus. Note that the under-compaction method resulted in general in denser samples in most cases, whereas the slurry method resulted in looser samples. Preparing the samples with these two different methods, apart from achieving different initial void ratios, the effect of the preparation method on the shear modulus component G_{vh} as well as the different moduli including G_{hv} and G_{hh} could be examined allowing a more systematic investigation into the fabric anisotropy of the samples. These two different preparation methods also represented roughly the material states from the dam (compacted tailing) to the pond (slurry state).

In total, eleven specimens were prepared and tested in the triaxial apparatus with bender elements. The characteristics of these specimens are summarized in Table 2. Note that the specimens with codes UB-S, MB-S and PO-S were prepared with the slurry method, where the first term (UB, MB, or PO) denotes the type of tailing soil used for the sample preparation. In addition, three specimens with codes UB-C, MB-C and PO-C were prepared with the under-compaction method. All these six specimens were tested in a fully saturated state applying typical procedures of saturation by checking the B value (Skempton's value) with subsequent steps of cell pressure and back pressure increase. Typically, the saturation of the specimens was assumed to be completed for a value of B greater than 0.95. Finally, an additional set of five specimens with codes UB-DRY01, UB- DRY02, UB-DRY03, MB-DRY and PO-DRY were prepared using the under-compaction method at variable initial densities, but tested with the bender elements in a dry state under variable confining

Table 2 Details of bender element testing program

	Test details		Measurement of modulus components			G_{vh} constants	
	e_0	Dry/Sat	G_{vh}	G_{hh}	G_{hv}	A (MPa)	n
UB-S	0.709	Sat	●	●	●	41.8	0.59
UB-C	0.540	Sat	●	●	●	36.5	0.59
UB-DRY01	0.464	Dry	●	–	–	34.7	0.57
UB-DRY02	0.623	Dry	●	–	–	42.3	0.57
UB-DRY03	0.502	Dry	●	–	–	34.4	0.60
MB-S	0.747	Sat	●	●	●	36.8	0.67
MB-C	0.739	Sat	●	●	●	42.2	0.56
MB-DRY	0.627	Dry	●	–	–	43.1	0.52
PO-S	0.872	Sat	●	●	●	38.1	0.64
PO-C	0.902	Sat	●	●	●	36.5	0.64
PO-DRY	0.795	Dry	●	–	–	44.9	0.54

pressures. For these specimens, volumetric strains and changes of void ratio were estimated based on the measurement of the sample axial strain from both an external vertically positioned LVDT and the local axial strain instrumentation as well as from the local radial strain LVDTs. For the six fully saturated specimens, their volumetric strains were principally measured directly from the back volume changes but with additional measurements of the deformation of the samples locally.

Details of the measurements with the vertical and lateral bender element configurations for the different components of shear modulus (G_{vh}, G_{hv} and G_{hh}) and the initial void ratios of the specimens (e_0) are given in Table 2. Note that all the tests were conducted applying an isotropic confining pressure to the specimen, thus the mean effective confining pressure is equal to $p' = \sigma'_a = \sigma'_r$, where σ'_a and σ'_r are the axial and radial effective stresses, respectively. The range of p' during the bender element test measurements varied from about 50 kPa to 680 kPa for most of the specimens.

3. RESULTS AND DISCUSSION

3.1 Typical Results of the Bender Element Tests

In Fig. 5, typical plots of the bender element tests signal analysis are given with respect to sample PO-C at p' = 200 kPa. Bender element tests were conducted in a range of frequencies typically between 7 to 10 kHz with respect to G_{vh} measurements (vertical bender elements instrumentation) and at slightly higher frequencies, typically between 10 to 20 kHz for G_{hv} and G_{hh} measurements (lateral bender elements instrumentation). These different ranges of frequencies were adopted for the conduction of the bender element tests in the vertical and horizontal directions, respectively, in order to ensure that the wavelength is less than half the distance between the bender element tips, which also assured better quality of the signal output (Youn *et al.* 2008). Typically, V_s ranged between about 100 m/s to 280 m/s for mean effective confining pressures from 100 kPa to 400 kPa. Note that a frequency of 10 kHz considering V_s = 200 m/s, would correspond to a wavelength of about 20 mm and that the distance between the tips in the vertical direction would be approximately equal to 88 to 92 mm for most specimens based on that the length of the bender element tip is about 3 mm and that some additional sample deformation takes place during the increase of the pressure. On the other hand, the distance between the bender element tips in the horizontal direction would be about 40 to 43 mm, approximately, which would require relatively greater frequencies to maintain a wavelength less than half in magnitude in comparison to the horizontal bender element tips. Note that using a pattern of frequencies, an averaged T_a was determined throughout this visual process over a range of frequencies for any given specimen to identify a consistent feature in the waves (Alvarado and Coop 2012).

For most samples, four to five different frequencies were applied for the subsequent measurement of G_{vh}, G_{hv} and G_{hh} and an averaged time arrival (T_a) was estimated for a given sample, confining pressure and mode of the bender element test (*i.e.*, G_{vh}, G_{hv} or G_{hh} measurement) within the whole spectrum of frequencies used. For all the tests, the first time arrival method was used for the measurement of V_s. An illustration of this process to derive averaged time arrival and compute the shear wave velocity and thus, the shear modulus, is given in Fig. 5. Note that, in general, the signal output from the bender element tests in the vertical direction (measurement of G_{vh}) was the strongest, and that the signal output for the measurement of G_{hv} was relatively stronger than the corresponding signal for the measurement of G_{hh} for most of the tests.

3.2 Discussion on Fabric Anisotropy and Sample Preparation Effects

Based on the measurement of shear modulus from the bender element tests, it was revealed that, for a given soil type and preparation method (or density), the samples had very similar values of the three different components of modulus, *i.e.*, $G_{vh} \approx G_{hv} \approx G_{hh}$, which demonstrates a fairly isotropic state. Typical plots comparing the different components of modulus based on the measurements with the lateral and vertical bender elements are given in Fig. 6 for the UB and MB samples tested in a fully saturated state. Note that the shear moduli of the specimens prepared with the under-compaction method have been multiplied by 4 in Fig. 6 in order to show clearly the different components of modulus separately for under-compacted specimens and specimens prepared with the slurry method. Note that Kuwano and Jardine (2002) found that stiffness anisotropy was seen in freshly formed air pluviated samples under isotropic confining stresses, reflecting their initially anisotropic fabrics. However that study did not discuss on particle shape effects since the studied material was clay. Yang *et al.* (2008) found that for dry pluviation method, no preferred orientation in the horizontal plane of the sample and they called it the transverse isotropy. In the vertical plane, the preferential particle orientation is in the horizontal direction, which was caused by gravitational forces during the deposition process which resulted from the sample preparation method. It can be considered that this is related to the elongated shape of the particles. Santamarina and Cho (2004) also reported that the fabric anisotropy is due to aligned non-spherical platy or ellipsoidal particles, even under isotropic confinement. In the present study, the S values are between about 0.6 ~ 0.7 and the R values are about 0.3, which means the particles are quite angular but not so elongated. Thus, it is possible that because of this, the fabric anisotropy is negligible no matter what preparation method is used.

In Fig. 7, the plots of shear modulus (using G_{vh} values) against (p') are given for the tailing silt MB comparing the two different methods of preparation; the slurry method against the under-compaction method. For this purpose, $G_{\max}$ values are normalized with respect to a void ratio function, $f(e) = e^{-1.29}$ (after Payan *et al.* 2016) to eliminate possible effects of the initial density. Within the scatter of the data, these results, which are representative for the whole set of experiments of the study, showed a relatively small effect of the preparation method by means of normalized modulus against pressure plots. The specimen prepared with the slurry method (MB-S) showed greater sensitivity to pressure expressed through a greater in magnitude power n, equal to 0.67, in comparison to the under-compacted specimens (MB-C and MB-DRY) with the latter showing values of the power n in the range of 0.52 to 0.56. As shown in the subsequent section, for the other types of tailing soils the values of the power n were much closer between specimens prepared with the under-compaction and the slurry methods.

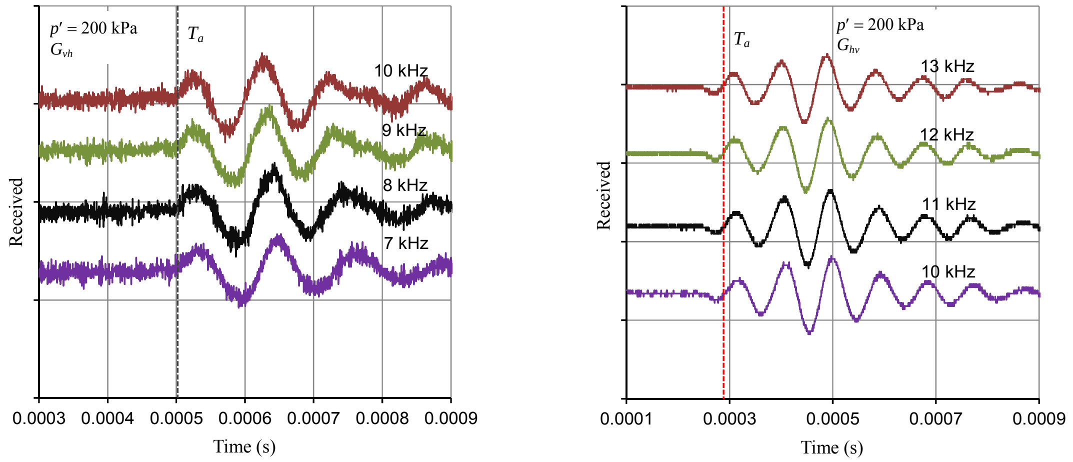

(a) Measurement of G_{vh} from vertical bender elements (b) Measurement of G_{hv} from lateral bender elements

Fig. 5 Typical plots of signal output from the bender element tests for specimen PO-C

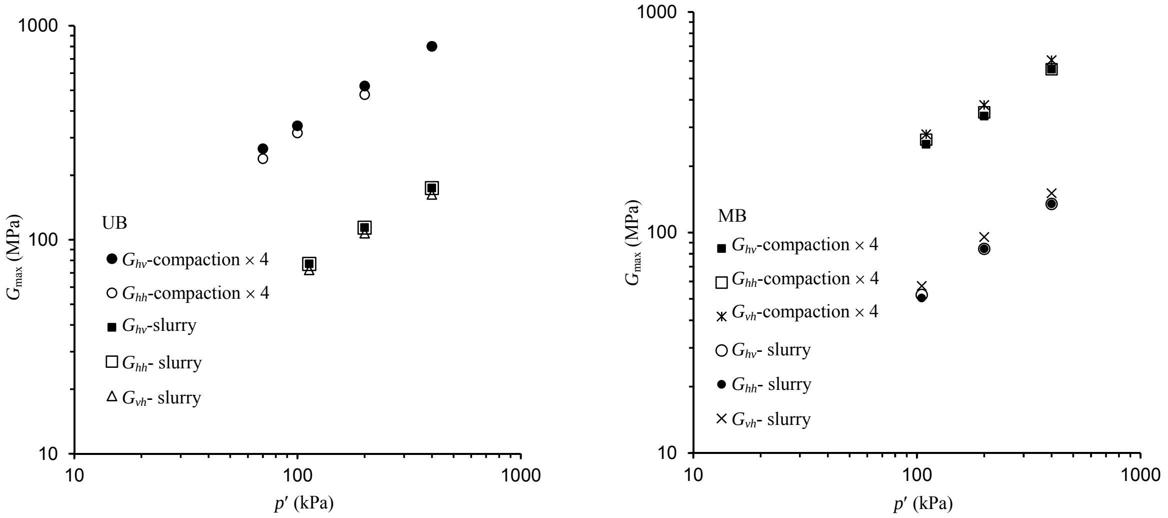

(a) For UB samples (b) For MB samples

Fig. 6 Typical plots of small-strain shear modulus against the mean effective confining pressure with vertical and lateral bender elements comparing the different components of modulus

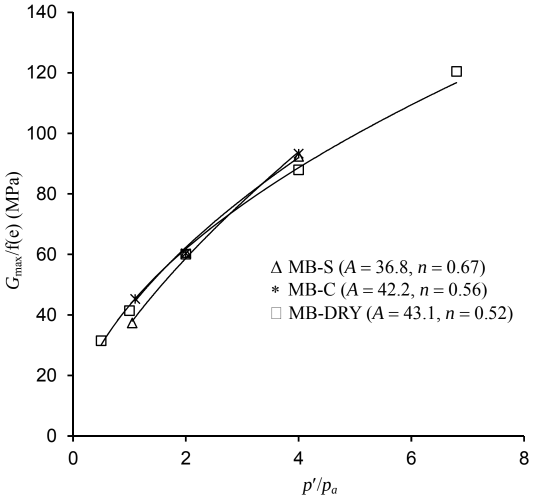

Fig. 7 Typical plots of normalized shear modulus with respect to a void ratio function against the normalized pressure comparing specimens constructed with different preparation method (the example corresponded to sample MB)

3.3 Sensitivity of Modulus to Pressure and Comparison with Literature Expressions for Quartz Sand

Soil modulus is expressed as a function of the mean effective confining pressure, typically with a power law type expression of the general form of Eq. (1) (Hardin and Richart 1963; Santamarina *et al*. 2001).

$$G_{\max} = A \times f(e) \times \left(\frac{p'}{p_a} \right)^n \tag{1}$$

Using the expression for $f(e)$ proposed by Payan *et al*. (2016), plotting $G_{\max}/f(e)$ against the normalized pressure (p'/p_a), where p_a = 100 kPa, the power (n) of Eq. (1) was estimated from a best fit of the power law type expression. All the estimated (n) values are summarized in Table 2. These values ranged from about 0.52 to 0.67 for the total set of experiments, which corresponded to sands of irregular shaped grains (Senetakis *et al*. 2012; Payan *et al*. 2016). Note that while Fig. 7 plots showed that there was some effect of the sample preparation on the shear modulus

– confining pressure relationship of the MB samples, the results of Table 2 did not show similar trends for the UB samples (UB-S versus UB-C) or the PO samples (PO-S versus PO-C).

In their study, Payan *et al.* (2016) quantified the effect of the coefficient of uniformity (C_u) and particle shape expressed with the regularity descriptor (ρ), on $G_{\max}$ model parameters (A) and (n) of Eq. (1) for quartz sands with the expressions of Eq. (2), where $G_{\max}$ of Eq. (1) is expressed in MPa in this case.

$$A = 84 \times C_u^{-0.14} \times \rho^{0.68} \tag{2a}$$

$$n = C_u^{0.12} \times (-0.23 \times \rho + 0.59) \tag{2b}$$

where C_u is the coefficient of uniformity and ρ is the particle shape descriptor of regularity.

In Fig. 8, this expression has been used to predict the $G_{\max}$ values of the tailing soils of the study incorporating their C_u and (ρ) values (Table 1). The estimated moduli are plotted against the measured values, using G_{vh} measurements. Even though the mineralogies of these tailing soils are very different with that of the quartz sands used to develop the expression of Eq. (1), the expression proposed by Payan *et al.* (2016) satisfactorily predicted the moduli of the samples for the whole range of densities and pressures of the study.

Payan *et al.* (2016) noticed that the predictive capacity of a $G_{\max}$ model should be evaluated not only by means of estimated against measured moduli plots, as for example it was implemented in Fig. 8, but also by means of normalized modulus against the state parameter. This is because small-strain modulus depends on the state of the soil. In soil mechanics, the state of the soil is expressed typically in terms of void ratio – confining pressure variables, but researchers have suggested the use of other sets of variables, for example overconsolidation ratio – confining pressure for clays (Viggiani and Atkinson 1995) or state parameter – confining pressure (Yang and Liu 2016). In Fig. 9, this type of evaluation is given, where the vertical axis corresponded to the normalized modulus taken as the ratio of the predicted against the measured moduli and the horizontal axis corresponded to the state parameter ξ expressed as (ξ + 1). Note that the value of ξ corresponds to the vertical distance of the current state of a soil in the void ratio-pressure plane to its critical state, *i.e.*, ξ is equal to $e - e_{cs}$, where e is the current void ratio and e_{cs} is the void ratio at the critical state (Been and Jefferies 1985). Note that the authors have conducted monotonic triaxial tests quantifying the critical state parameters of the three tailing soils which results have not been included in this article (Li 2017). Based on the measurements of the state parameter of the samples for each given pressure the bender element tests were conducted and the estimated versus the measured moduli, the results of Fig. 9 were produced. These results along with the results of Fig. 8 demonstrated that the expression of $G_{\max}$ from Eqs. (1) and (2), derived on the basis of quartz type sands (Payan *et al.* 2016), predicted within satisfactory limits the moduli of the tailing soils, even though a scatter was observed of the order of ±20% between measured and predicted moduli. It is interesting to notice that even though the expression proposed by Payan *et al.* (2016) was developed from experiments on medium grained to coarse grained sands in a relatively narrow range of coefficients of uniformity and that their experiments were conducted on pure-quartz type sands, the predictive capacity of that model is demonstrated to be satisfactory for the iron tailings of the study, which had a diversity of minerals and sizes from silt to sand. This implies that in predicting the modulus of tailing non-plastic soils, perhaps a careful examination of the grains to quantify the particle shape could be a first step, even though the satisfactory estimation of the modulus of the three iron tailing of the study from the expression developed by Payan *et al.* (2016), does not imply that this satisfactory prediction must be the case for other types of non-plastic tailings.

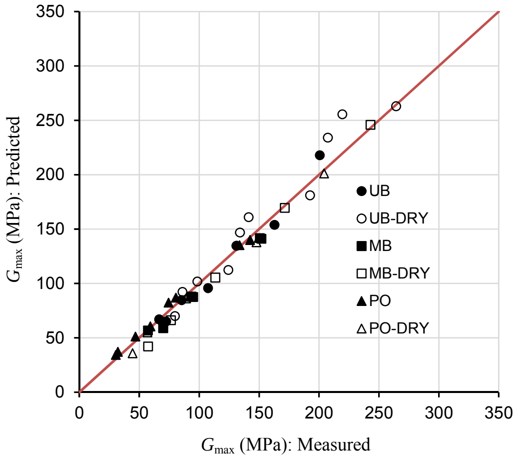

Fig. 8 Comparison of measured values of G_{vh} against predicted using an expression proposed by Payan *et al.* (2016) for quartz type sands

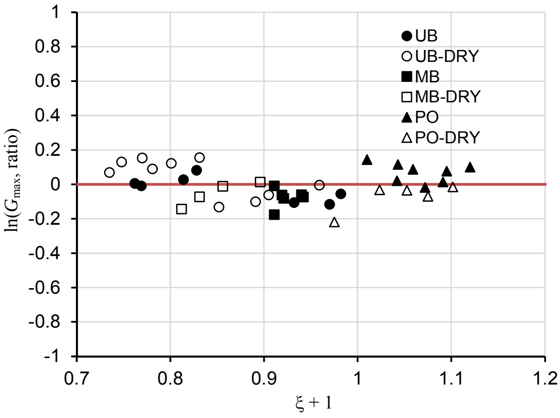

Fig. 9 Performance of a literature expression (Payan *et al.* 2016) in predicting the modulus of the tailing soils by means of the ratio of predicted over measured values against the state parameter

4. CONCLUSIONS

The study reported on the small-strain shear modulus of three soils taken from the Panzhihua tailing dam in China. These three soils are classified as iron tailings with size from silt to sand. Basic characterization of the materials was based on XRD analysis for the quantification of the basic minerals of the soils and SEM analysis. The SEM images were used to quantify the particle shape descriptors of the grains which were subsequently used in the analysis of the modulus of the soils. Three different modulus components were measured; G_{vh} based on vertical bender elements and G_{hv}, G_{hh} based on lateral bender elements. The data showed that samples prepared with the under-compaction or slurry methods, had similar moduli, whilst the analysis of the vertical and lateral bender elements showed isotropic behavior. Interestingly, an expression proposed in the literature developed on the basis on experiments on quartz type sands predicted within satisfactory limits the behavior of the tailing soils. This evaluation was conducted by means of predicted against measured values and by means of the state parameter.

ACKNOWLEDGEMENTS

The work described in this paper was fully supported by a grant from the Research Grants Council of the Hong Kong Special Administrative Region, China Project No. 9041880 (CityU 112813). The authors would like to acknowledge the anonymous reviewers for their constructive comments and detailed suggestions that helped us to improve the quality of the manuscript.

NOTATIONS

d_{50}	mean particle size (mm)
d_{60}	particle size at 60% passing (mm)
d_{30}	particle size at 30% passing (mm)
d_{10}	particle size at 10% passing (mm)
C_u	coefficient of uniformity
C_c	coefficient of curvature
G_s	specific gravity
ξ	state parameter
ρ	regularity
e	void ratio
e_0	initial void ratio
e_{cs}	void ratio at critical state
$G_{\max}$	maximum shear modulus (MPa)
G_{vh}	$G_{\max}$ from the bender element tests which propagated vertically and polarised horizontally the shear waves (MPa)
G_{hv}	$G_{\max}$ from the bender element tests which propagated horizontally and polarised vertically the shear waves (MPa)
G_{hh}	$G_{\max}$ from the bender element tests which both propagated and polarised horizontally the shear waves (MPa)
R	roundness
S	sphericity
p'	mean effective stress (kPa)
p_a	atmospheric pressure (= 100 kPa)
V_s	shear wave velocity (m/s)

REFERENCES

Alvarado, G. and Coop, M.R. (2012). "On the performance of bender elements in triaxial tests." *Géotechnique*, **62**(1), 1–17.

Been, K. and Jefferies, M.G. (1985). "A state parameter for sands." *Géotechnique*, **35**(2), 99–112.

Bishop, A.W. and Wesley, L.D. (1975). "A hydraulic triaxial apparatus for controlled stress path testing." *Géotechnique*, **25**(4), 657–670.

Cho, G.C., Dodds, J., and Santamarina, J.C. (2006). "Particle shape effects on packing density, stiffness, and strength: Natural and crushed sands." *Journal of Geotechnical and Geoenvironmental Engineering*, **132**(5), 591–602.

Clayton, C.R.I. (2011). "Stiffness at small strain: Research and practice." *Géotechnique*, **61**(1), 5–37.

Davies, M.P. and Lighthall, P.C. (2001). "Geotechnical aspects of several recent mine tailings impoundment failures." *Proceedings of 54th Canadian Geotechnical Conference*, 321–326.

Hardin, B. and Richart, F. (1963). "Elastic wave velocities in granular soils." *Journal of the Soil Mechanics and Foundations Division*, ASCE, **89**, 33–65.

Ishihara, K. (1993). "Liquefaction and flow failure during earthquakes." *Géotechnique*, **43**(3), 351–451.

Ishihara, K. (1996). *Soil Behaviour in Earthquake Geotechnics*. Oxford Science Publications.

Kramer, S.L. (1996). *Geotechnical Earthquake Engineering*. Pearson Education India.

Krumbein, W.C. and Sloss, L.L. (1963). *Stratigraphy and Sedimentation*. 2nd Ed., Freeman and Company, San Francisco.

Kuwano, R. and Jardine, R.J. (2002). "On the applicability of cross-anisotropic elasticity to granular materials at very small strains." *Géotechnique*, **52**(10), 727–749.

Ladd, R.S. (1978). "Preparing test specimens using undercompaction." *Geotechnical Testing Journal*, **1**(1), 16–23.

Li, W. (2017). *The Mechanical Behaviour of Tailings*. Ph.D. Dissertation, City University of Hong Kong.

Payan, M., Khoshghalb, A., Senetakis, K., and Khalili, N. (2016). "Effect of particle shape and validity of $G_{\max}$ models for sand: A critical review and a new model." *Computers and Geotechnics*, **72**, 28–41.

Richart, F.E., Hall, J.R., and Woods, R.D. (1970). *Vibrations of Soils and Foundations*. Prentice Hall, Englewood Cliffs, 414pp.

Robertson, P.K. (2010). "Evaluation of flow liquefaction and liquefied strength using the cone penetration test." *Journal of Geotechnical and Geoenvironmental Engineering*, **136**(6), 842–853.

Santamarina, C., Klein, K., and Fam, M. (2001). *Soils and Waves*. John Wiley and Sons, New York.

Santamarina, J.C. and Cho, G.C. (2004). "Soil behavior: The role of particle shape." *Proceedings of the Skempton Conference*, March, London UK.

Senetakis, K., Anastasiadis, A., and Pitilakis, K. (2012). "The small-strain shear modulus and damping ratio of quartz and volcanic sands." *Geotechnical Testing Journal*, **35**(6), 964–980.

Viggiani, G. and Atkinson J.H. (1995). "Stiffness of fine-grained soil at very small strains." *Géotechnique*, **45**(2), 249–65.

Wise Uranium Project (WISE) (2014). Chronology of major tailing dam failures, website: http://www.wise-uranium.org/mdaf.html.

Yang, Z.X., Li, X.S., and Yang, J. (2008). "Quantifying and modelling fabric anisotropy of granular soils." *Géotechnique*, **58**(4), 237–248.

Yang, J. and Liu, X. (2016). "Shear wave velocity and stiffness of sand: The role of non-plastic fines." *Géotechnique*, **66**(6), 500–514.

Youn, J.-U., Choo, Y.-W., and Kim, D.-S. (2008). "Measurement of small-strain shear modulus $G_{\max}$ of dry and saturated sands by bender element, resonant column and torsional shear tests." *Canadian Geotechnical Journal*, **45**, 1426–1438.